Selectivity, Kinetics, and Efficiency of Reversible Anion Exchange with TcO_4^- in a Supertetrahedral Cationic Framework

Shuao Wang, Ping Yu, Bryant A. Purse, Matthew J. Orta, Juan Diwu, William H. Casey, Brian L. Phillips, Evgeny V. Alekseev, Wulf Depmeier, David T. Hobbs, and Thomas E. Albrecht-Schmitt**

$[ThB_5O_6(OH)_6][BO(OH)_2]\cdot 2.5H_2O$ (Notre Dame Thorium Borate-1, NDTB-1) is an inorganic supertetrahedral cationic framework material that is derived from boric acid flux reactions. NDTB-1 exhibits facile single crystal to single crystal anion exchange with a variety of common anions such as Cl^-, Br^-, NO_3^-, IO_3^-, ClO_4^-, MnO_4^-, and CrO_4^{2-}. More importantly, NDTB-1 is selective for the removal of TcO_4^- from nuclear waste streams even though there are large excesses of competing anions such as Cl^-, NO_3^-, and NO_2^-. Competing anion exchange experiments and magic-angle spinning (MAS)-NMR spectroscopy of anion-exchanged NDTB-1 demonstrate that this unprecedented selectivity originates from the ability of NDTB-1 to trap TcO_4^- within cavities, whereas others remain mobile within channels in the material. The exchange kinetics of TcO_4^- in NDTB-1 are second-order with the rate constant k_2 of 0.059 s^{-1} M^{-1}. The anion exchange capacity of NDTB-1 for TcO_4^- is 162.2 mg g^{-1} (0.5421 mol mol^{-1}) with a maximum distribution coefficient K_d of 1.0534×10^4 mL g^{-1}. Finally, it is demonstrated that the exchange for TcO_4^- in NDTB-1 is reversible. TcO_4^- trapped in NDTB-1 can be exchanged out using higher-charged anions with a similar size such as PO_4^{3-} and SeO_4^{2-}, and therefore the material can be easily recycled and reused.

1. Introduction

Because of its high fission yield (≈6.03%) from ^{235}U, the radionuclide ^{99}Tc is present as a large inventory in nuclear waste at most storage sites. It is estimated that there is approximately 305 metric tons (≈190 PBq) of ^{99}Tc that has been generated from both nuclear reactors and weapons testing from 1943 to 2010.[1] ^{99}Tc is a β emitter with a long half-life of 2.13×10^5 years. As a result, ^{99}Tc is one of the most important radiotoxicity contributors during long-term waste storage. Unlike its congener MnO_4^-, TcO_4^- is not a strong oxidant and is relatively unreactive. Technetium is therefore present mainly as TcO_4^- under a large range of conditions from strongly oxidative to even mildly reductive environments.[2] TcO_4^- is highly soluble and extremely mobile in aqueous systems. The velocity of TcO_4^- transportation in the subsurface was determined to be almost the same as that of groundwater.[3] In addition, compared to some other water-soluble radionuclides from fission such as ^{137}Cs and ^{90}Sr, TcO_4^- is much more unlikely to be sorbed by the soil in repositories.[4] Finally, the volatile nature of some Tc(VII) compounds (e.g., Tc_2O_7) that are generated during nuclear waste vitrification makes technetium problematic in the off-gas system design for vitrification facilities.[2] The combination of

S. Wang, B. A. Purse, M. J. Orta, J. Diwu, Prof. T. E. Albrecht-Schmitt
Department of Chemistry and Biochemistry and
Department of Civil Engineering and Geological Sciences
156 Fitzpatrick Hall
University of Notre Dame
Notre Dame, IN 46556, USA
E-mail: talbrec1@nd.edu

Dr. P. Yu
NMR Facility
University of California-Davis
One Shields Ave, Davis, CA 95616, USA

Prof. W. H. Casey
Department of Chemistry
University of California-Davis
One Shields Ave, Davis, CA 95616, USA
E-mail: whcasey@ucdavis.edu

Prof. B. L. Phillips
Department of Geosciences
SUNY-Stony Brook
Stony Brook, NY 11794-2100, USA

Dr. E. V. Alekseev
Forschungszentrum Jülich GmbH
Institute for Energy and Climate Research (IEK-6)
Jülich 52428, Germany

Prof. W. Depmeier
Institut für Geowissenschaften
Universität zu Kiel
Kiel 24118, Germany

Dr. D. T. Hobbs
Savannah River National Laboratory
Aiken, SC 29808, USA

DOI: 10.1002/adfm.201103081

TcO_4^- mobility in groundwater and technetium volatility during vitrification increases the risk of the offsite release of ^{99}Tc.

Currently, the major inventory of TcO_4^- in the United States is present mostly in high-level nuclear waste stored at the Hanford Site in eastern Washington and the Savannah River Site in South Carolina. Most of the ^{99}Tc is present in the water-soluble fraction of the high level waste and is not removed by pretreatment processes that capture ^{137}Cs, ^{90}Sr, and α-emitting radionuclides. The decontaminated or low-activity waste (LAW) solutions containing ^{99}Tc are incorporated into a grout waste-form at the Savannah River Site and will likely be incorporated into a borosilicate glass wasteform at Hanford.[5] Effective removal of TcO_4^- from the LAW stream prior to vitrification would eliminate problems associated with volatilization during the vitrification process.

At least two strategies for the technetium separation have already been proposed. One is using commercially available anion exchange resins to remove TcO_4^- from the LAW stream before vitrification[6] and the other is using a strong reducing agent such as zero-valent iron to reduce TcO_4^- to lower valent technetium species (e.g., TcO_2), which have much lower solubility in aqueous solutions and are much less volatile.[7] At Hanford, the separated ^{99}Tc would be vitrified in the high-activity waste (HAW) melter. At present, a decision has not been made concerning the best method to remove or process the TcO_4^- in the LAW stream. First, both the efficiency and the selectivity for removing TcO_4^- in the LAW are poor especially for the commercially available anion exchange resins. Second, both separation strategies mentioned above would require processing either TcO_4^--loaded ion-exchange materials or technetium-containing eluant into the HAW melter resulting in a volume increase for the HAW glass wasteform. Technetium volatility would likely be an issue in the HAW melter unless technetium can be isolated from both LAW and HAW completely and incorporated in its own suitable waste form.

During the last two decades, significant efforts have been made in designing materials for removing TcO_4^- from nuclear waste solutions with better selectivity and efficiency. Among these, several novel organic polymer-based bifunctional anion-exchange resins with high exchange selectivity towards TcO_4^- have been reported.[8] However, associated with their organic nature, the thermal and chemical stability along with resistance to radiation damage for these resins are very limited. Furthermore, large excess of these exchange materials are used in TcO_4^- exchange, which questions the selectivity of the materials.

To address these drawbacks, a series of inorganic anion-exchangable materials have been prepared, which are mostly represented by the hydrotalcite clays, also known as layered double hydroxides (LDHs), and its analogues.[9] LDHs have been shown to exchange with a variety of anions including TcO_4^- for the anions (usually halide, nitrate, or carbonate) that originally reside in its interlayer space.[10] However, carbonate has proven to have the strongest affinity in LDHs, which leads to a poor exchange selectivity towards TcO_4^-.[11] Very recently, Oliver and co-workers discovered a series of cationic materials with weakly bonded 1,2-ethanedisulfonate anions that undergo rapid anion exchange and examples of these include SLUG-21 and SLUG-26.[12–14] In particular, SLUG-21 shows a high exchange capacity and affinity towards MnO_4^-, which would show potential applications to selectively remove TcO_4^- from waste solutions, although it still contains organic-based fragments.[13]

We recently reported the synthesis and crystal structure of a purely inorganic supertetrahedral cationic framework material, $[ThB_5O_6(OH)_6][BO(OH)_2]\cdot 2.5H_2O$ (Notre Dame Thorium Borate-1, **NDTB-1)**, which has fascinating anion exchange capabilities, and the ^{99}Tc-magic-angle spinning (MAS)-NMR spectroscopy of the TcO_4^- exchanged **NDTB-1** material showing TcO_4^- can be trapped in the cavities of **NDTB-1**, which might lead to unprecedented exchange selectivity.[15,16] Here, we will re-emphasize the synthesis and the structural features of **NDTB-1**. We then report the details for the anion exchanges (mainly for TcO_4^-) of **NDTB-1** including exchange kinetics, exchange capacity, and the distribution coefficient, K_d. We also demonstrate the exchange selectivity using a series of anion exchange competing experiments and MAS-NMR spectroscopy on the anion-exchanged **NDTB-1** materials. Finally, we present the TcO_4^- removal experiments using a simulated Hanford low-activity melter recycle stream, which demonstrates that **NDTB-1** can be used to remove TcO_4^- in the presence of potentially competing anions such as nitrate, nitrite, and chloride.

2. Synthesis and Structural Features of NDTB-1

NDTB-1, with the formula $[ThB_5O_6(OH)_6][BO(OH)_2]\cdot 2.5H_2O$, can be synthesized from boric acid flux reactions with $Th(NO_3)_4\cdot 5H_2O$ or $ThOCO_3$ at 200 °C. **NDTB-1** is obtained as a pure phase with in 72.8% yield based on Th. This can be confirmed by powder X-ray diffraction data (Figure S1, Supporting Information). However, the morphology of the crystals is greatly improved by starting with $ThOCO_3$ instead of $Th(NO_3)_4\cdot 5H_2O$.

The crystal structure of **NDTB-1** is a porous supertetrahedral 3D framework that crystallizes in the $Fd\,\bar{3}$ space group. The building blocks of this framework are twelve-coordinate Th^{4+} polyhedra surrounded by BO_3 triangles and BO_4 tetrahedra. The BO_4 tetrahedra chelate the thorium centres, while the BO_3 groups share vertices with thorium polyhedra. Almost regular icosahedral coordination geometry is found for the thorium atoms. The borate units are polymerized and form $B_{10}O_{24}$ clusters with three-fold symmetry that bridge between the thorium atoms, which results in a supertetrahedral framework structure shown in **Figure 1**a.

Thorium atoms and crown-like $B_{10}O_{24}$ groups do not fill all of the space in the supertetrahedra and, as a consequence of this architecture, a system of channels and cavities are observed in the structure of **NDTB-1**. The channels extend along cubic [110] directions (Figure 1a) and intersect in the center of the supertetrahedra to form cavities with four equivalent gates (Figure 1b). The gates into the intersecting chambers in the cavities have a hexagonal form with the size of 9.4 Å × 7.8 Å (Figure 1c). The free void volume percentage in **NDTB-1** is very high at 43%, which makes it the second most porous actinide compound known.[17] A combination of single crystal X-ray diffraction (XRD), charge-balance considerations, and ^{11}B MAS NMR spectroscopy shows that this supertetrahedral framework possesses a positive charge with disordered protonated BO_3 units (i.e., $H_2BO_3^-$) in the channels and cavities.[15]

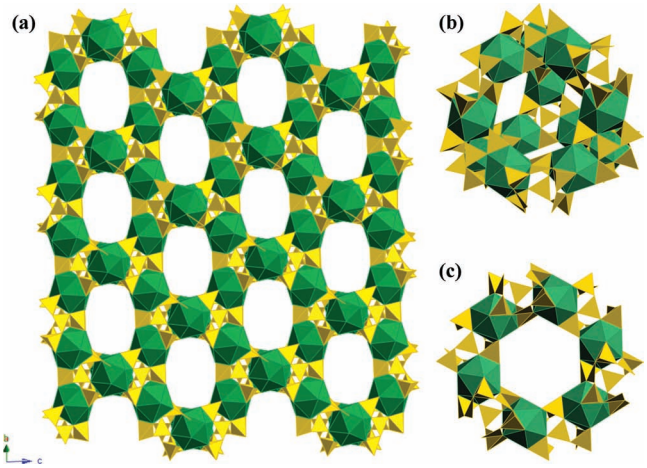

Figure 1. a) A view of the supertetrahedral framework structure of **NDTB-1** with channels through cubic <110> directions. Th polyhedra are shown in green and borate are shown in yellow. b) Depiction of a supertetrahedral cavity formed by four hexagonal windows (gates). c) A view of hexagonal windows (gates).

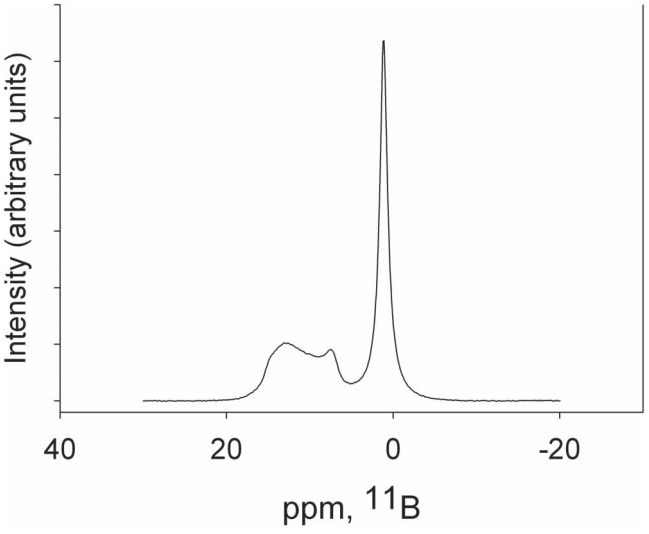

Figure 2. ^{11}B-MAS-NMR powder pattern of **NDTB-1** at 160.45 MHz and 15 kHz spinning rate. The sharp peak near 0 ppm corresponds to tetrahedral borate. The broad, two-horned peak near 15 ppm corresponds to trigonal boron and has at least two sites. The integrated intensities of these two peaks gives the ratio of BO_3 to BO_4 of 0.82(5).

All these structural features make **NDTB-1** one of the best candidates for applications of selective anion exchange. First, boric acid is a very weak acid with the first pK_a of 9.23. As a result, $H_2BO_3^-$ anions that originally reside within the structure readily hydrolyze back to H_3BO_3 in aqueous solutions under a wide range of pH. Other anions therefore tend to enter the structure of **NDTB-1** required by the principle of charge-balance. Second, $H_2BO_3^-$ is unbound to the cationic framework and the interaction between the two is solely provided by weak Coulombic forces. Third, within the cationic framework, the channels form a network that pierces the whole structure and allows facile anionic transport for the exchange processes. Finally, the cavities are able to trap the anions with suitable charge and size. Exchange selectivity is therefore provided based on the fact that small anions are mobile in the channels while larger anions are not able to enter the structure.

3. ^{11}B-MAS-NMR Spectra of NDTB-1

Solid-state ^{11}B MAS NMR spectra show distinct signals from well-ordered BO_3 and BO_4 groups, as found from the single-crystal XRD data. The ordered BO_3 groups yield a characteristic MAS powder pattern with horns that correspond to the steep edge near +15 ppm and the peak at +7.5 ppm, best fit with an isotropic chemical shift $\delta = 17.5$ ppm and quadrupolar coupling parameters $C_q = 2.65$ MHz, $\eta = 0$ (**Figure 2**). However, a powder pattern for a well-ordered site cannot account for the broad area of intensity from 14 to 10 ppm, between the sharper BO_3 features. This intensity can be explained by the presence of additional BO_3 environments that experience a distribution of electric-field gradients. Such additional features are in accord with the presence of a disordered BO_3 group as was suspected from the crystal structure. The ratio of BO_3 to BO_4 integrated intensity, 0.82(5), far exceeds that expected from the 2:3 crystallographic ratio of the framework and provides further support for the existence of additional, extra-framework BO_3 groups.

To better resolve the sources of this broad area of intensity, we collected multi-quantum magic-angle spinning (MQMAS) spectra of the material, the BO_3 region of which is shown in **Figure 3**. The full ^{11}B MQMAS spectrum also contains a narrow, symmetric peak for tetrahedrally coordinated boron at $F1 = 1.3$, $F2 = 0.6$ ppm that is omitted from Figure 3 for clarity. The BO_3 region of the MQMAS spectrum contains multiple resolved signals and highlights the disordered nature of the corresponding BO_3 groups as was inferred from the MAS spectrum. The disordered BO_3 groups yield a broad peak in the isotropic dimension, centered near F1 = 19 ppm, corresponding to a correlated distribution of isotropic chemical shifts and quadrupolar coupling constants with decreasing intensity from $\delta = 17$ ppm and $C_q = 2.55$ MHz to $\delta = 14.5$ ppm and $C_q = 2.35$ MHz. The ordered framework BO_3 groups give a sharp $F1$ peak at 20.8 ppm and well-defined quadrupolar powder pattern in the anisotropic dimension (Figure 3 inset, middle). The MQMAS spectrum also shows a third BO_3 signal at $F1 = 21.9$ ppm that is not resolved in the MAS spectrum. In the anisotropic dimension (Figure 3 inset, bottom), this third peak shows an unusual, smoothed $F2$ lineshape that is not accompanied by a diagonal ridge of intensity that would be expected for a distribution of C_q values from structural disorder. The cause of this peak shape is uncertain, but could be relatively low-frequency, restricted motions, perhaps indicating the presence of more loosely bound BO_3 groups in the channels. Signals from apparently mobile groups were observed in NMR spectra of most anions exchanged into **NDTB-1** (see below). These ^{11}B-NMR data are consistent with a model of the **NDTB-1** structure with several sites for boron, including ordered BO_4 and BO_3 sites in the framework along with two other disordered BO_3 groups that experience a range of local structures

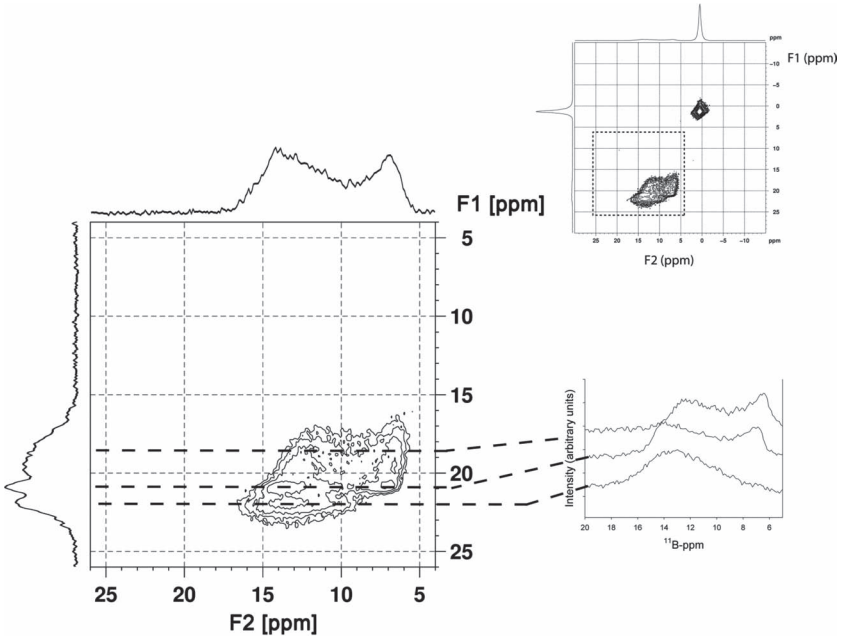

Figure 3. Contour plot of a ^{11}B MQMAS NMR spectrum (ν_R = 35.0 kHz, 11.74 T) of the **NDTB-1** material. The spectra at left and top are summed projections of the *F1* (isotropic) and *F2* (anisotropic) dimensions, respectively, and the upper inset shows both a sharp signal near 0 ppm (0.6 ppm in *F2*, +1.3 ppm in *F1*) corresponding to tetrahedrally coordinated boron ($B(O)_4$) and the broader signal at higher ppm values corresponds to trigonal boron (17–23 ppm in *F2*, 10–5 ppm in *F2*). This BO_3 region is expanded in the larger figure at the left and shows the presence of three distinct BO_3 signals. The lower inset shows *F2*-cross sections taken at the peak maxima in *F1* at 21.9, 20.8, and 18.7 ppm, from bottom to top, respectively. The spectrum was acquired at spectral widths of 16.6 kHz (*F2*) and 35 kHz (*F1*) with 96 scans per slice. The three-pulse zero-quantum filter sequence was employed with 2.4 μs excitation and 0.78 μs conversion pulses at a 250 kHz RF field followed by a 56 μs selective 90° pulse.

as expected for sites in the channels and cavities. The existence of these extra-framework BO_3 moieties is consistent with the results of anion-exchange experiments (see below).

4. Anion Exchange Properties of NDTB-1

Anion exchange experiments of **NDTB-1** were conducted with a variety of common anions including halides (Cl^-, Br^-, I^-), and oxoanions such as MnO_4^-, TcO_4^-, ReO_4^-, PO_4^{3-}, CrO_4^{2-}, $Cr_2O_7^{2-}$, SO_4^{2-}, SeO_4^{2-}, SeO_3^{2-}, ClO_4^-, NO_3^-, and IO_3^-. The anion exchange experiments were confirmed by the combination of techniques including combined inductively coupled plasma mass spectrometry (ICP-MS), energy-dispersive X-ray spectroscopy (EDS), and UV-vis-NIR absorption spectroscopy. As determined by single-crystal and powder XRD of anion-exchanged **NDTB-1** materials, the whole structure remains intact throughout the exchange process (Figure S1, Supporting Information). More impressive is the fact that single crystals retain their integrity throughout the exchange, which results in a rare phenomenon of single crystal to single crystal anion exchange, although disordering of the exchanged anions in the channels remains a crystallographic problem. This is critical for the reusability of **NDTB-1** and contrasts sharply with the fact that most of LDH structures collapse after the exchange.[9c] Exchange experiments conducted with a variety of highly colored anions, such as MnO_4^-, CrO_4^{2-}, and $Cr_2O_7^{2-}$, can result in the single crystals showing the color of the transition metal anions within a few minutes (**Figure 4**). UV-vis-NIR spectra were also collected for these colored anion exchanged crystals, which further demonstrate the presence of the colored anions in the crystals (Figure S2, Supporting Information).

The critical anion exchange experiments involve replacing the extraframework borate anions with TcO_4^-. The uptake of the TcO_4^- by **NDTB-1** was monitored using the charge-transfer bands (290 nm) in the UV region of the spectrum. In order to derive the exchange kinetics, large excesses of **NDTB-1** were used. In particular, 10 mg of **NDTB-1** and 3 mL of a solution containing 1.455×10^{-4} M TcO_4^- were mixed in a cuvette without shaking. UV-vis spectra were acquired every 20 min for 7 days to probe the concentration of TcO_4^- in solution as a function of time. These studies of as-synthesized intact crystals of **NDTB-1** show

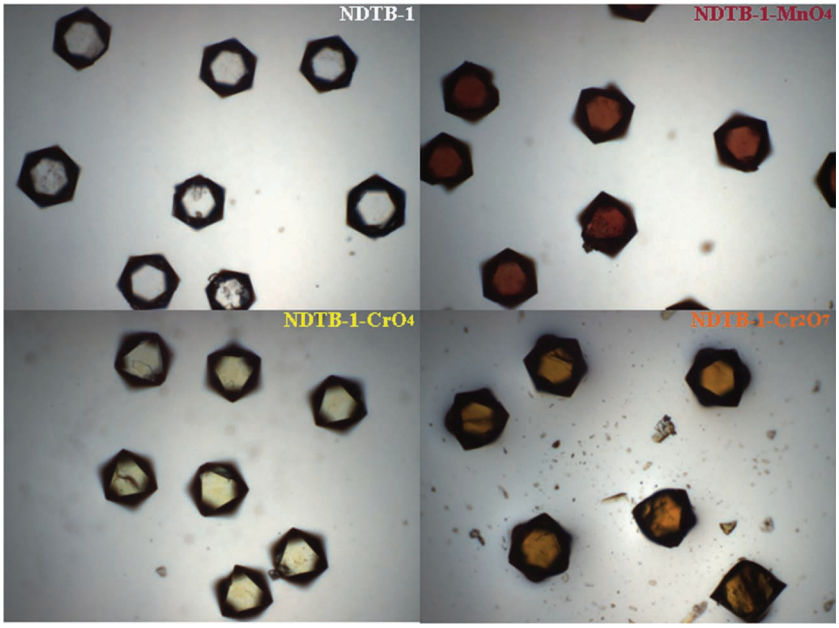

Figure 4. Photographs of crystals of **NDTB-1**, MnO_4^- exchanged **NDTB-1**, CrO_4^{2-} exchanged **NDTB-1**, and $Cr_2O_7^{2-}$ exchanged **NDTB-1**.

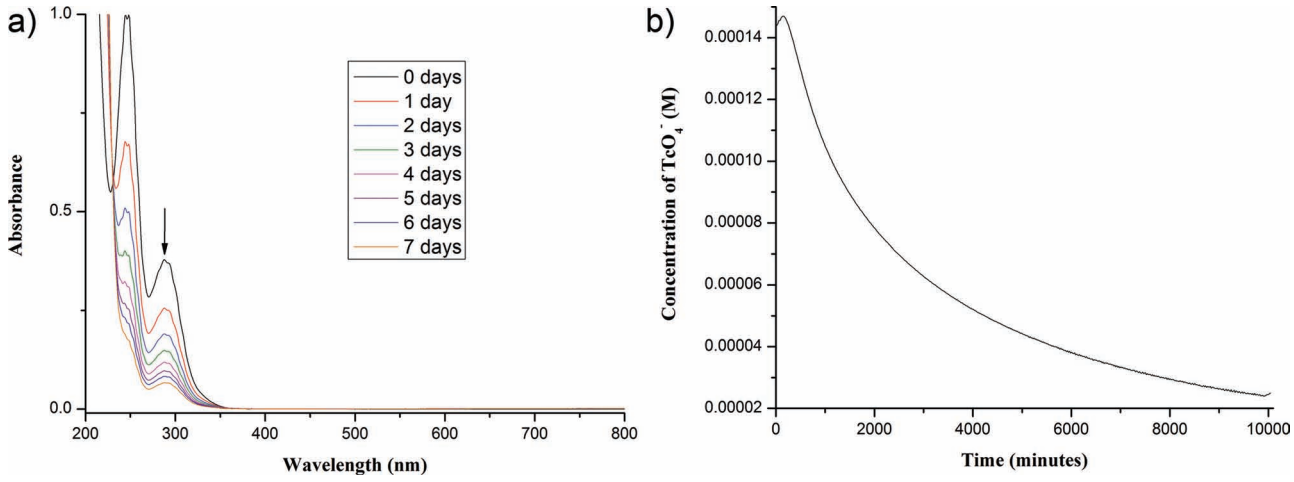

Figure 5. a) UV-vis spectra of TcO_4^- solution exchanged with **NDTB-1.** b) Plot of concentrations of TcO_4^- concentration as a function of exchange time.

rapid uptake of TcO_4^- from solution show in **Figure 5**a (in day width) and the plots for the concentration of TcO_4^- as a function of exchange time is shown in Figure 5b. The plot of 1/concentration for TcO_4^- as a function of time was also examined (Figure S3, Supporting Information), where a proper linear fit can be applied. This is consistent with the fact that the exchange reaction is a second-order reaction with TcO_4^-. The rate law for the TcO_4^- exchange reaction could be therefore described as:

$$v = \mathrm{d}c(\mathrm{TcO_4^-})/\mathrm{d}t = kc(\mathrm{TcO_4^-})^2 \quad (1)$$

assuming **NDTB-1** is always in excess, where the rate constant k is the slope of the linear fit plot and was calculated to be 0.059 s^{-1} M^{-1}.

The exchange capacity of **NDTB-1** for TcO_4^- was also examined using a series of exchange reactions with different molar ratios of TcO_4^- to **NDTB-1**. In particular, six different molar ratios (1:1, 1:2, 1:4, 1:8, 1:16, 1:32) were selected and their exchange curves are shown in **Figure 6**. In the 1:1 exchange reaction, a maximum of about 54.21% of TcO_4^- could be removed from the solution (**Table 1**). When the amount of **NDTB-1** was doubled, the maximum amount of TcO_4^- that was removed from solution increases sharply to 83.62%. Further increasing the amount of **NDTB-1** did not result in a significant improvement for TcO_4^- removing. About 96.07% of TcO_4^- was found to be removed in the 1:32 reaction. The maximal exchange capacity of **NDTB-1** can be calculated in the 1:1 reaction to be 162.2 mg g^{-1} and 0.5421 mol mol^{-1}. However, to achieve a better exchange completeness, a small excess of **NDTB-1** is required.

In addition, the exchange results can also be described by the exchange coefficients K_d, which can be defined as:

$$K_d(\mathrm{mL\ g^{-1}}) = \frac{\text{Equilibrium mass of Tc exchanged into NDTB}-1}{\text{Equilibrium mass of Tc in solution}} \times \left(\frac{\text{Volume of solution}}{\text{Mass of NDTB} - 1}\right) \quad (2)$$

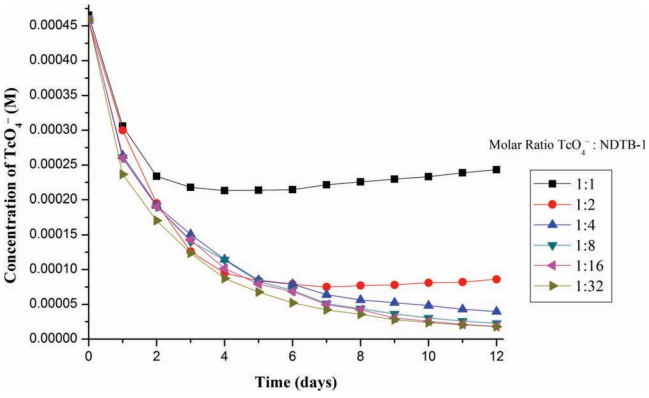

Figure 6. Plots of concentrations of TcO_4^- concentration as a function of time for reactions with six different molar ratios of TcO_4^- to **NDTB-1**.

The maximal K_d value is found in the 1:4 reaction to be 1.0534×10^4 mL g^{-1} (Table 1), which is significantly higher than any other anion exchange materials known to date and thus a new record is provided for TcO_4^- removal.[10,18]

Table 1. Results of studies on exchange capacity and exchange efficiency of **NDTB-1.**

Molar ratio TcO_4^-:NDTB-1	Maximal percentage of TcO_4^- removed[a)] [%]	Exchange capacity[b)] [mol mol^{-1}]	Final percentage of TcO_4^- removed [%]	K_d[c)] [mL g^{-1}]
1:1	54.21	0.5421	47.75	3656
1:2	83.62	0.4181	81.14	8604
1:4	91.33	0.2283	91.33	10534
1:8	95.08	0.1188	95.08	9663
1:16	96.01	0.0600	96.01	6016
1:32	96.07	0.0300	96.07	3056

[a)]Maximal percentages of TcO_4^- removed are calculated using the lowest concentration of TcO_4^- monitored during the exchange reactions; [b)]Exchange capacity = moles of maximal removed TcO_4^-/moles of **NDTB-1** that used; [c)]Exchange coefficients are calculated using the formula of (2).

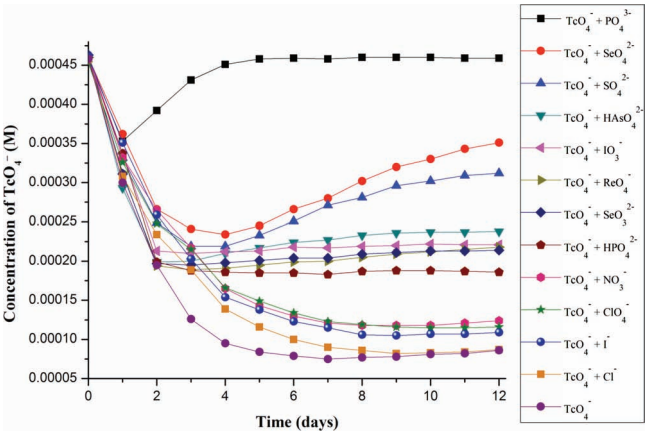

Figure 7. Plots of concentrations of TcO_4^- concentration as a function of time for 13 different reactions with or without competing anions.

Table 2. Results of studies on exchange selectivity of **NDTB-1**.

Anions	Maximal percentage of TcO_4^- removed [%]	Final percentage of TcO_4^- removed [%]	K_d [mL g^{-1}]
TcO_4^-	83.62	81.14	8604
$TcO_4^- + Cl^-$	81.98	81.06	8560
$TcO_4^- + I^-$	77.28	76.26	6424
$TcO_4^- + ClO_4^-$	74.61	74.41	5816
$TcO_4^- + NO_3^-$	74.37	72.89	5377
$TcO_4^- + HPO_4^{2-}$	60.01	59.32	2916
$TcO_4^- + SeO_3^{2-}$	57.97	53.83	2332
$TcO_4^- + ReO_4^-$	58.87	52.61	2220
$TcO_4^- + IO_3^-$	54.46	52.02	2168
$TcO_4^- + HAsO_4^{2-}$	56.64	48.34	1871
$TcO_4^- + SO_4^{2-}$	52.70	32.66	970
$TcO_4^- + SeO_4^{2-}$	49.23	23.72	622
$TcO_4^- + PO_4^{3-}$	23.08	0	0

5. Anion Exchange Selectivity of NDTB-1

The anion exchange selectivity of **NDTB-1** was probed by a series of TcO_4^- exchange reactions with different kinds of secondary competing anions. Twelve competing anions (Cl^-, I^-, ClO_4^-, NO_3^-, HPO_4^{2-}, SeO_3^{2-}, ReO_4^-, IO_3^-, $HAsO_4^{2-}$, SO_4^{2-}, SeO_4^{2-}, and PO_4^{3-}) were selected based on several considerations: first, none of these anions are able to produce transitions in the wavelength range used for identification of TcO_4^- in the UV-vis spectra; second, there should be no redox reaction involving the competing anions and TcO_4^-; and third, these anions provide wide distributions of size, configuration, and charge, therefore, the factors that determine the selectivity of **NDTB-1** can be examined. To address the drawback of using large excesses of anion exchange materials, which might hide the real selectivity, a molar ratio of TcO_4^-:competing anion:**NDTB-1** = 1:1:2 was strictly applied for all exchange reactions. The pH was also monitored for all reactions in the final to examine the effects of carbonate (Table S1, Supporting Information).

The exchange selectivity can be derived based on the comparison of the exchange kinetics and the exchange coefficients of TcO_4^- with different kinds of competing anions. In particular, the anions with a better ability to slow the exchange kinetics and decrease the exchange coefficient of TcO_4^- has a larger affinity for being exchanged into **NDTB-1**. The exchange curves of TcO_4^- for all reactions are shown in **Figure 7** and the exchange results are listed in **Table 2**. It is not surprising that the TcO_4^- exchange reaction without competing anions has the largest removal percentage and K_d value. Based on the distribution of final percentages of TcO_4^- removed and K_d values, we can simply divide these 12 competing exchange reactions into four groups.

The first group contains reactions of $TcO_4^- + Cl^-$, $TcO_4^- + I^-$, $TcO_4^- + ClO_4^-$, and $TcO_4^- + NO_3^-$. These reactions still have relatively high TcO_4^- exchange and K_d values, although these values are slightly smaller than those for the pure TcO_4^- exchange (Table 1). These four competing anions share a common feature in that they are all –1 charged anions and much smaller than TcO_4^-. It also can be found that their competing abilities are strongly associated with their sizes. For example, Cl^- is the smallest anion and essentially does not compete with TcO_4^- for exchange based on the K_d value. The other three anions are slightly larger and possess better competing abilities.

The second group consists of HPO_4^{2-}, SeO_3^{2-}, ReO_4^-, IO_3^-, and $HAsO_4^{2-}$ as the competing anion. It has to be noted that although HPO_4^{2-}, SeO_3^{2-}, and $HAsO_4^{2-}$ was used as starting materials, based on the pH (Table S1, Supporting Information), their actual species in solution are dominated by $H_2PO_4^-$, $HSeO_3^-$, and $H_2AsO_4^-$, respectively. Thus, all of these anions share a common character that they are all –1 charged anions and very close to TcO_4^- in size (based on M–O bond distances in the anions). A reasonable prediction that TcO_4^- and ReO_4^- should share almost the same affinity for being exchanged into **NDTB-1** can be made based on the fact that they are almost identical in both charge and size.[2] This prediction is also supported by comparing K_d values between the competing reaction with molar ratio TcO_4^-:ReO_4^-:**NDTB-1** of 1:1:2 and the reaction with molar ratio of TcO_4^-:**NDTB-1** of 1:1 (Table 1 and 2). A deduction of this prediction is that the competing anions showing a better competing ability than ReO_4^- would also outcompete with TcO_4^- for being exchanged into **NDTB-1**.

The third group includes competing anions of SO_4^{2-} and SeO_4^{2-}, which are both –2 charged anions. It was observed that both anions outcompete with TcO_4^- for being exchanged into **NDTB-1**. In addition, SeO_4^{2-} is significantly larger than SO_4^{2-} and possesses a better competing ability than SO_4^{2-}, as observed between Cl^- and I^-, as well as $H_2PO_4^-$ and $H_2AsO_4^-$. More importantly, TcO_4^- exchange into **NDTB-1** is reversible, i.e., TcO_4^- that is initially exchanged into **NDTB-1** is further exchanged back into solution using anions such as SeO_4^{2-}. From here, a conclusion can be derived that the anion exchange selectivity of **NDTB-1** is based on both the size and the charge of the anions. Anions with larger size and charge will possess better affinity for being exchanged into **NDTB-1**.

The last group only contains PO_4^{3-} as the competing anion. Interestingly, this competing reaction shows a completely

reversible exchange for TcO_4^- after one day. All TcO_4^- that initially exchanged into **NDTB-1** is further exchanged back into solution, which results in the K_d value being zero. It should be noted that the pH monitored at the end of this reaction is 7.92 (Table S1, Supporting Information). Although PO_4^{3-} is added initially, it is rapidly protonated and HPO_4^{2-} becomes the dominant species at this pH. However, based on the previous conclusion, the fact that HPO_4^{2-} is close to SO_4^{2-} in size is not consistent with the completely reversible exchange. We propose that this completely reversible exchange is the consequence of a combination of two factors. First, excess of HCO_3^- should be present under these conditions, which could compete with TcO_4^- for exchange. Second, although HPO_4^{2-} is the dominate species in solution, the equilibrium between HPO_4^{2-} and PO_4^{3-} still exists. Accordingly, PO_4^{3-} is favored for being trapped in **NDTB-1**, which would shift the equilibrium in the solution towards PO_4^{3-} without significantly changing the pH because the borate that exchanged out from **NDTB-1** is a good buffer in the pH range from 7.4 to 9.2. The later factor could play a major role, since HCO_3^- should not be considered as a good competing anion based on the previous conclusion.

As a summary, the priority order for being exchanged into **NDTB-1** can be listed as:

$Cl^- < I^- \approx ClO_4^- \approx NO_3^- < H_2PO_4^- < HSeO_3^- \approx TcO_4^- \approx ReO_4^- \approx IO_3^- < H_2AsO_4^- < SO_4^{2-} < SeO_4^{2-} < PO_4^{3-}$

6. MAS-NMR Studies of Anion-Exchanged NDTB-1 Materials

The phosphate- and tellurate-exchanged **NDTB-1** samples show two, and possibly three, signals in NMR spectra (**Figure 8**). The ^{31}P NMR spectra exhibited a strong, narrow signal at 2.3 ppm, and a broader shoulder spanning the 0 to –11 ppm range. The signal at 2.3 ppm becomes narrower at higher spinning rates, possibly because of increased frictional heating of the rotor, while the weak broad signal at 0 to –11 ppm does not change. The ^{125}Te NMR spectra display only a strong signal at 1086 ppm, together with a broader group of signals in the 1102–1190 ppm range (the ^{125}Te standard is crystalline ZnTe, chemical shift at –888 ppm). None of these signals vary with spinning rate. The SeO_4^{2-} and ClO_4^--loaded **NDTB-1** exhibited only a single sharp peak in the respective ^{77}Se and ^{35}Cl NMR spectra. Although, the ^{35}Cl-MAS-NMR spectra contained a sharp peak near 0 ppm relative to the ClO_4^- external standard, a large background signal from the probe might have obscured any additional ^{35}Cl-NMR peaks. No NMR signal could be confidently resolved for ^{55}Mn in the MnO_4^--exchanged material because of a large ^{55}Mn background signal.

The ^{99}Tc MAS-NMR spectra (**Figure 9**) indicate two distinct signals, with a possible third signal. The two most conspicuous signals have isotropic chemical shifts at near +0 ppm and upfield, in a range from –8 to –40 ppm. The downfield peak is sharp and narrow and diminishes profoundly in intensity with decreasing temperature. The characteristics of this sharp peak are consistent with those of the TcO_4^- anion.

The conspicuous upfield signal is much broader, does not diminish in intensity with temperature (Figure 9), and

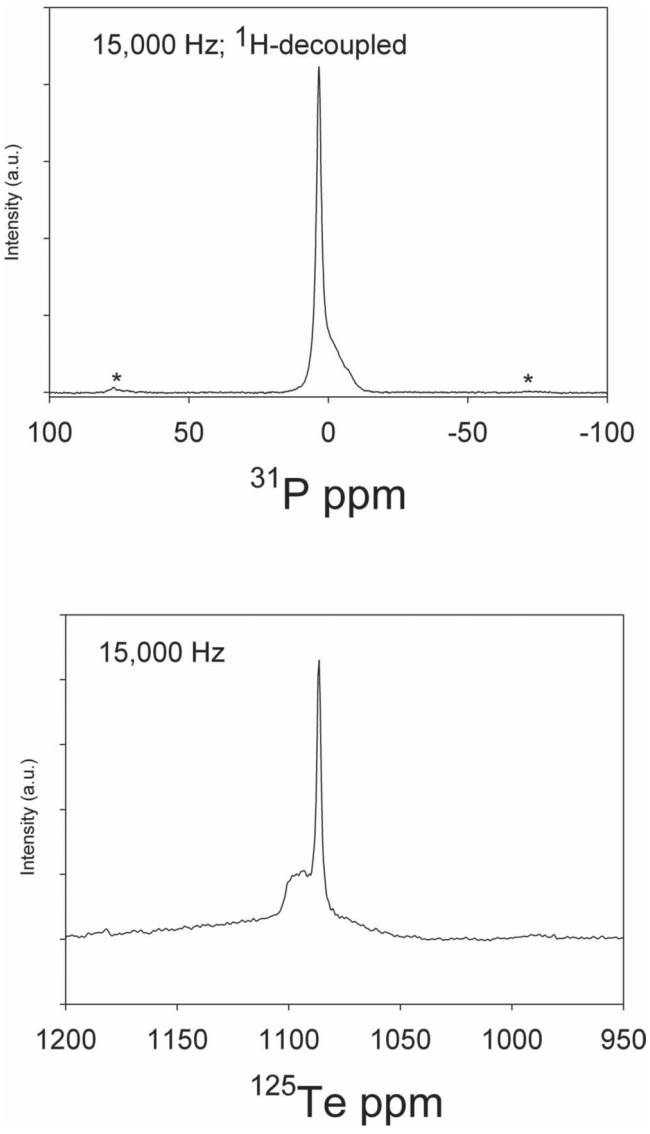

Figure 8. ^{31}P- and ^{125}Te-MAS-NMR spectra of anion-exchanged **NDTB-1** material containing phosphate (top) and tellurate (bottom).

exhibits spinning sidebands at all temperatures (weak peaks separated from the main peak by ±15 kHz). This broad peak could be fit with a second-order quadrupolar powder pattern for a single site with $\delta = -39$ ppm, $C_q \approx 0.16$ MHz, $\eta_q = 0$ (from a least-squares of the spectrum at 223 K), by including sufficient line broadening to smooth the fine-structure. The spectra and parameters are consistent with an interpretation that the chemical environment around the ^{99}Tc nucleus is disturbed by bonding to the cationic framework. Furthermore, the ^{99}Tc-NMR intensity contained in the conspicuous spinning sidebands indicates assignment to a dynamically rigid species, in contrast to the narrow downfield peak where evidence suggests mobility.

The relative intensity of the two major peaks (–39 and +0.1 ppm) are estimated by integrating signals from the low-temperature data. The smaller peak has about 6% (±1.5%) of the total intensity, so they differ in relative intensities by a ratio of ≈20:1 at 193 K.

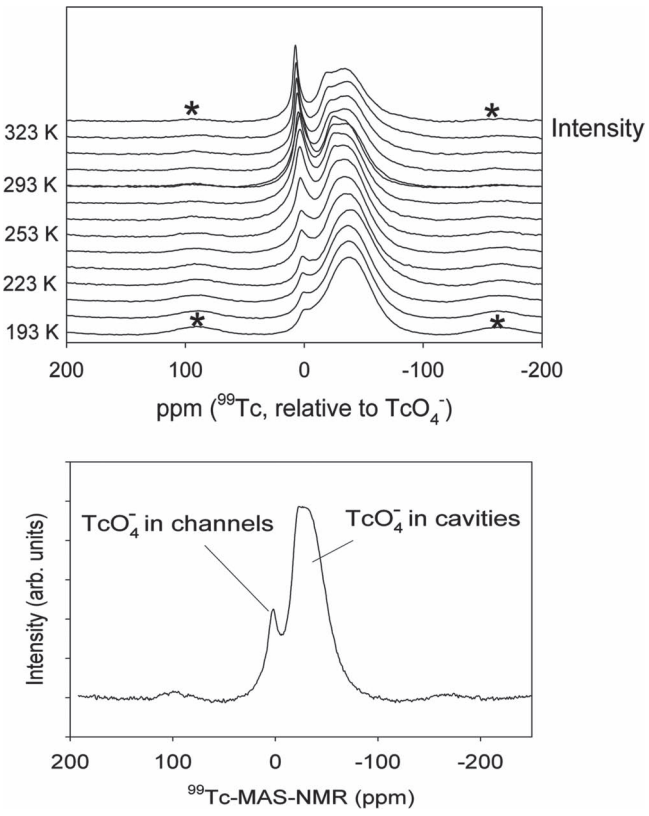

Figure 9. Top panel: A variable-temperature series of ^{99}Tc-MAS-NMR spectra showing two clear sites, one of which becomes less prominent as temperature decreases. Bottom panel: The assignment of these two signals is a $^{99}TcO_4^-$ ion in a channel that can tumble freely at all but the lowest temperatures. The freedom to tumble, and thus the peak intensity near 0 ppm, declines with temperature. The upfield peak exhibits an intensity that does not change appreciably with temperature and is interpreted to correspond to a $^{99}TcO_4^-$ site bound more tightly to the framework.

The declining intensity of this narrow peak with decreasing temperature is interpreted to indicate that the molecule is dynamically averaging the ^{99}Tc transitions into a narrow signal at room temperature. As the sample cools, the dynamic averaging diminishes, causing intensity from the satellite transitions to be lost from the single peak and broadened into the baseline.

Fine structure is evident in this peak near –20 ppm from ca. 298 K to 323 K (Figure 9) that resembles second-order quadrupolar broadening, however, the fact that the narrow feature appears to broaden as temperature is further reduced suggests instead the presence of a small amount of mobile TcO_4^- in the cages. Some time variation in the intensities of the two most conspicuous peaks is observed, with the intensity of the narrow downfield peak growing with time over six weeks. The slow change in relative intensities of the ^{99}Tc signals indicates that movement between the two sites is much slower than the NMR time scale.

These results are consistent with the idea that both the channels and the cages in the **NDTB-1** are taking up TcO_4^- (aq) to balance the net cationic charge of the framework. The TcO_4^- in the channels gives rise to the narrow peak near 0 ppm in the spectra. The broader upfield peak is assigned to TcO_4^- in the cavities and accounts for most of the signal.

Table 3. Composition of simulated Hanford LAW melter recycle stream.

Anion	Concentration [M]	Anion:TcO_4^- Mole Ratio
TcO_4^-	1.94×10^{-4}	1.0
NO_3^-	6.07×10^{-2}	314
Cl^-	6.39×10^{-2}	330
NO_2^-	1.69×10^{-1}	873
SO_4^{2-}	6.64×10^{-6}	0.0343
CO_3^{2-}	4.30×10^{-5}	0.222

7. TcO_4^- Removal from a Simulated Hanford LAW Melter Recycle Stream

The simulated Hanford LAW melter recycle stream used in this test was composed of four anions, NO_3^-, NO_2^-, Cl^-, and CO_3^{2-}, in addition to TcO_4^-. Three of the anions, NO_3^-, NO_2^-, and Cl^-, are present in large excess with respect to TcO_4^-, with mole ratios ranging from 314–873 (**Table 3**). The predominant cation in the simulant is Na^+ with smaller concentrations of NH_4^+, K^+, and Ca^{2+}. Given the large molar excess of NO_3^-, NO_2^-, and Cl^-, this solution represents a significant challenge to an ion exchange material for the effective removal of TcO_4^-.

Despite the high concentration of potentially competing anions, TcO_4^- removal was observed upon contact of the simulant with **NDTB-1** at phase ratios of 200 and 40 mL g^{-1}. At a phase ratio of 200 mL g^{-1}, 13.0% of the ^{99}Tc was removed after a 4-hour batch contact at ambient temperature. At a phase ratio of 40 mL g^{-1}, 44.8% of the ^{99}Tc was removed at the same conditions. From the measured ^{99}Tc removal, the calculated K_d values are 2.99×10^1 and 1.62×10^1 mL g^{-1} at the phase ratios of 200 and 40 mL g^{-1}, respectively. The low K_d values are not unexpected given the chemical composition of the simulated waste solution. Nevertheless, the test findings indicate that **NDTB-1** serves as a highly selective ion exchanger for TcO_4^- from a solution containing between two and three orders of magnitude higher concentrations of NO_3^-, NO_2^-, and Cl^-.

8. Conclusions

In conclusion, we have discovered a unique material, **NDTB-1**, that shows extensive potential applications for removing pertechnetate from nuclear waste streams. This material possesses an ability to remove TcO_4^- from aqueous solutions with both unprecedented selectivity and greatly improved efficiency. Furthermore, **NDTB-1** is highly stable during the anion exchange processes thus provides a significant reusability for real applications. More importantly, the completely reversible exchange of TcO_4^- that observed in the exchange reaction using PO_4^{3-} as the competing anion provides a good opportunity for isolating TcO_4^- from both LAW and HAW. One can simply use the material to remove TcO_4^- until its exchange capacity is reached, then take the material off-line, and exchange out the TcO_4^- with SeO_4^{2-} or PO_4^{3-}. The separated TcO_4^- can then be reduced to a lower oxidation state and immobilized. A cycle is present in **Figure 10** that should solve the ^{99}Tc problem in nuclear waste.

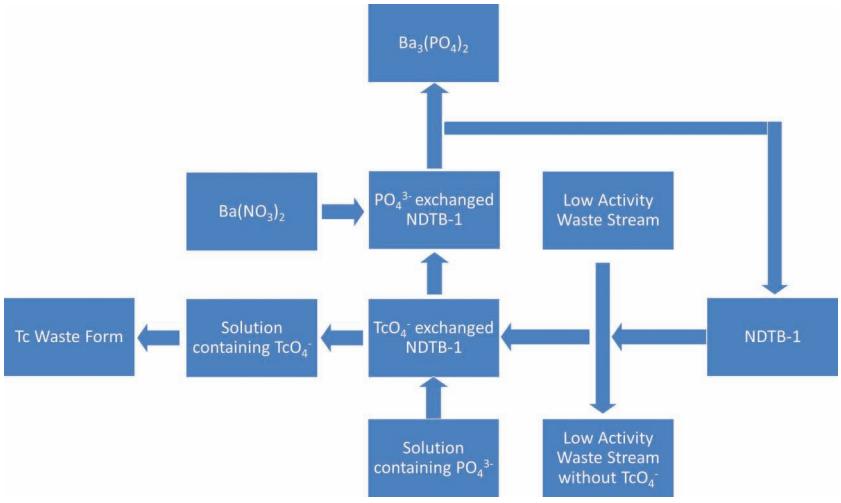

Figure 10. A scheme for recycling **NDTB-1**.

9. Experimental Section

Synthesis of NDTB-1: The procedure for making **NDTB-1** was reported previously.[15] Typically, $Th(NO_3)_4{\cdot}4H_2O$ (0.2000 g), boric acid (0.6717 g), and deionized (DI)-water (90 mL) were loaded into a 23 mL autoclave. The autoclave was sealed and heated to 200 °C in a box furnace for 7 days. The autoclave was then cooled to 160 °C at a rate of 1 °C h^{-1} followed by cooling at a rate of 9 °C h^{-1} to the room temperature. The product was washed with boiling water to remove excess boric acid. Crystals in the form of octahedra and their fragments could be isolated. Single crystal X-ray diffraction and powder X-ray diffraction studies revealed that **NDTB-1** could be made as a pure phase with a yield of 72.8% based on Th (Figure S1, Supporting Information).

Exchange Kinetics Studies of NDTB-1: 50 mg of TcO_2 was reacted with a large excess of 30% H_2O_2 to yield a solution containing TcO_4^-. 10 mg of **NDTB-1** material and 3 mL of a solution containing 1.455×10^{-4} M TcO_4^- was mixed in a cuvette without shaking. UV-vis spectra were acquired using a Cary 6000i spectrometer every 20 min for 7 days to probe the concentration of TcO_4^- in solution as a function of time.

Exchange Capacity and Exchange Coefficient Studies of NDTB-1: Six parallels of solutions (3 mL) containing 4.58×10^{-4} M TcO_4^- were mixed, respectively, with six **NDTB-1** samples with six different TcO_4^-:**NDTB-1** molar ratios of 1:1 (0.75 mg), 1:2 (1.5 mg), 1:4 (3 mg), 1:8 (6 mg), 1:16 (12 mg), and 1:32 (24 mg) in cuvettes without shaking. UV-vis spectra were acquired using a Cary 6000i spectrometer at same time every day for 12 days to probe the concentration of TcO_4^- in solution as a function of time.

Exchange Selectivity Studies of NDTB-1: Twelve parallels of solutions (1.5 mL) containing 9.16×10^{-4} M TcO_4^- and solutions (1.5 mL) containing 9.16×10^{-4} M competing anions (Cl^-, I^-, ClO_4^-, NO_3^-, HPO_4^{2-}, SeO_3^{2-}, ReO_4^-, IO_3^-, $HAsO_4^{2-}$, SO_4^{2-}, SeO_4^{2-}, and PO_4^{3-}) were mixed respectively with **NDTB-1** (1.5 mg) with TcO_4^-:competing anion:**NDTB-1** molar ratios of 1:1:2 in cuvettes without shaking. UV-vis spectra were acquired using a Cary 6000i spectrometer at same time every day for 12 days to probe the concentration of TcO_4^- as a function of time.

Exchange Experiments with Simulated Hanford LAW Melter Recycle Stream and NDTB-1: A simulated Hanford LAW melter recycle stream was prepared using reagent grade chemicals and ultrapure water (MilliQ Element) composed of the following anions, Cl^-, NO_3^-, NO_3^-, SO_4^{2-}, CO_3^{2-}, and TcO_4^-. The molar concentration of the anions and molar ratio of each anion to that of TcO_4^- is provided in Table 3. Measured quantities of the simulated Hanford recycle stream were pipetted into plastic centrifuge tubes containing a premeasured quantity of **NDTB-1** to provide phase ratios of 200 mL g^{-1} (Expt 1) and 40 mL g^{-1} (Expt 2). A control test contained the simulant only. The centrifuge tubes were tightly stoppered and tumbled for 4 h at ambient laboratory temperature. The test suspension was filtered through a 0.10 µm syringe filter (Millex) and the clear filtrate collected in a clean polyethylene sample bottle. ^{99}Tc activity in the filtrate was determined by scintillation counting. A blank test served as the control to determine the ^{99}Tc in the untreated simulant and to ensure ^{99}Tc was not removed by sorption to the tube or filter media or by precipitation during the 4-h test period.

MAS-NMR Studies of Anion-Exchanged NDTB-1 Materials: The anion exchanged **NDTB-1** materials for MAS-NMR studies were prepared by the parallel anion exchange reactions using 200 mg **NDTB-1** each with 5 mL solutions containing 50 mg of TcO_4^-, $H_2PO_4^-$, ClO_4^-, SeO_4^{2-}, MnO_4^-, and TeO_4^{2-} for approximately 7 days. The anion exchanged **NDTB-1** materials were then washed with DI-water and dried at 65°C for 5 h. MAS-NMR spectra were collected on a Bruker AVANCE spectrometer equipped with a widebore 11.7 Tesla magnet, corresponding to ν_o = 202.446 MHz for ^{31}P, 123.91 MHz for ^{55}Mn, 157.782 MHz for ^{125}Te, 112.56 MHz for ^{99}Tc and 95.40 MHz for ^{77}Se, respectively. For ^{99}Tc-NMR, 1.3 µs nonselective pulses, a 5 s relaxation delay, and a 62.5kHz spectral window were used. Experiments conducted with the relaxation delay time varying from 1 to 15 s showed that 5 s is long enough to prevent any signal saturation. The spectra were obtained by summation of 64 transients and processed with 200 Hz of line broadening. The chemical shift is referenced to TcO_4^- solution (sealed in a quartz tube) at 0 ppm. ^{31}P MAS NMR data were collected with 15 kHz and 30 kHz spinning rates and single-pulse excitation with, and without, proton-decoupling sequences. Proton decoupling made no important difference in the spectra. In a typical experiment, 45° pulses and 60 s relaxation delays were used. The chemical shift was externally referenced to 85% H_3PO_4 at 0 ppm. ^{125}Te MAS-NMR data were collected with 12 and 15 kHz spinning rates, 45° pulses, and 60 s relaxation delays. The chemical shift was externally reference to crystalline ZnTe at –888 ppm. For ^{77}Se NMR, the pulse length was 1.7 µs (corresponding to 60° tip angle), the recycle delay time was 60 s, the number of transients was 960. The chemical shift was externally referenced to saturated H_2SeO_3 solution at 1288 ppm. Spectra were also collected on a **NDTB-1** loaded with ClO_4^- as the ion-exchanged species.

Supporting Information

Supporting Information is available from the Wiley Online Library or from the author.

Acknowledgements

This material is based upon work supported as part of the Materials Science of Actinides, an Energy Frontier Research Center funded by the U.S. Department of Energy, Office of Science, Office of Basic Energy Sciences under Award Number DE-SC0001089.

Received: December 19, 2011
Published online: March 20, 2012

[1] J. P. Icenhower, N. P. Qafoku, J. M. Zachara, W. J. Martin, *Am. J. Sci.* **2010**, *310*, 721.
[2] J. G. Darab, P. A. Smith, *Chem. Mater.* **1996**, *8*, 1004.
[3] M. J. Rudin, C. Stanton, R. G. Patterson, R. S. Garcia, *National Low-Level Waste Management Program Radionuclide Report Series*, vol. *2*,

Technetium-99, Idaho National Engineering Laboratory Technical Report DOE/LLW-118, INEL, Idaho Falls, ID, 1992.
[4] R. E. Wildung, T. R. Garland, K. M. McFadden, C. E. Cowan, in *Technetium in the Environment*, (Eds: G. Desmet, C. Myttenaera), Elsevier Science Publishing Co., New York **1986**, pp. 115–129.
[5] W. W. Lukens, D. A. Mckeown, A. C. Buechele, I. S. Muller, D. K. Shuh, I. L. Pegg, *Chem. Mater.* **2007**, *19*, 559.
[6] a) L. Liang, B. Gu, X. Yin, *Sep. Technol.* **1996**, *6*, 111; b) B. Gu, K. A. Dowlen, L. Liang, J. L. Clausen, *Sep. Technol.* **1996**, *6*, 123; c) G. D. Del Cul, W. D. Bostick, D. R. Trotter, P. E. Osborne, *Sep. Sci. Technol.* **1993**, *28*, 551.
[7] J. G. Darab, A. B. Amonette, D. S. D. Burke, R. D. Orr, S. M. Ponder, B. Schrick, T. E. Mallouk, W. W. Lukens, D. L. Caulder, D. K. Shuh, *Chem. Mater.* **2007**, *19*, 5703.
[8] a) B. Gu, G. M. Brown, P. V. Bonnesen, L. Liang, B. A. Moyer, R. Ober, S. D. Alexandratos, *Environ. Sci. Technol.* **2000**, *34*, 1075; b) P. V. Bonnesen, G. M. Brown, S. D. Alexandratos, L. Bates Bavoux, D. J. Presley, V. Patel, R. Ober, B. A. Moyer, *Environ. Sci. Technol.* **2000**, *34*, 3761.
[9] a) V. Rives, *LDHs: Layered Double Hydroxides: Present and Future*, Nova Science Publishers Inc., Hauppauge, NY **2001**; b) D. G. Evans, R. C. T. Slade, in *Layered Double Hydroxides*, (Ed: X. Duan, D. G. Evans), Springer-Verlag, New York **2006**; c) S. R. Oliver, *Chem. Soc. Rev.* **2009**, *38*, 1868.
[10] Y. F. Wang, H. Z. Gao, *J. Colloid Interface Sci.* **2006**, *301*, 19.
[11] S. Miyata, *Clays Clay Miner.* **1983**, *31*, 305.
[12] H. Fei, D. L. Rogow, S. R. J. Oliver, *J. Am. Chem. Soc.* **2010**, *132*, 7202.
[13] H. Fei, M. R. Bresler, S. R. J. Oliver, *J. Am. Chem. Soc.* **2011**, *133*, 11110.
[14] H. Fei, S. R. J. Oliver, *Angew. Chem. Int. Ed.* **2011**, *50*, 9066.
[15] S. Wang, E. V. Alekseev, J. Diwu, W. H. Casey, B. L. Phillips, W. Depmeier, T. E. Albrecht-Schmitt, *Angew. Chem. Int. Ed.* **2010**, *49*, 1057.
[16] P. Yu, S. Wang, E. V. Alekseev, W. Depmeier, T. E. Albrecht-Schmitt, B. L. Phillips, W. H. Casey, *Angew. Chem. Int. Ed.* **2010**, *49*, 5975.
[17] a) E. V. Alekseev, S. V. Krivovichev, W. Depmeier, *Angew. Chem. Int. Ed.* **2008**, *47*, 549; b) K. M. Ok, J. Sung, G. Hu, R. M. J. Jacobs, D. O'Hare, *J. Am. Chem. Soc.* **2008**, *130*, 3762; c) R. E. Wilson, S. Skanthakumar, K. E. Knope, C. L. Cahill, L. Soderholm, *Inorg. Chem.* **2008**, *47*, 9321.
[18] S. D. Balsley, P. V. Brady, J. L. Krumhansl, H. L. Anderson, *J. Soil Contam.* **1998**, *7*, 125.